Journal of Groundwater Science and Engineering
ISSN 2305-7068
Indexed by ESCI CABI CSA
Scopus GeoRef AJ CNKI

Adsorption mechanism of flumequine onto kaolinite: Evidence from density functional theory calculations and the effects of Cu(II)

Yan-dan Li, Bing-bing Li, Dan Zhang, Hong-han Chen, Hai-jiao Xie, Er-ping Bi

Citation:
Li YD, Li BB, Zhang D, Chen HH, Xie HJ, Bi EP. 2026. Adsorption mechanism of flumequine onto kaolinite: Evidence from density functional theory calculations and the effects of Cu(II). Journal of Groundwater Science and Engineering, 14(4): 478-492.

View online: https://doi.org/10.26599/JGSE.2026.9280090

Articles you may be interested in

Impact of Cr(III) complexation with organic acid on its adsorption in silts and fine sands
Journal of Groundwater Science and Engineering. 2024, 12(4): 347-359 https://doi.org/10.26599/JGSE.2024.9280026

Natural brown coal as an adsorbent for manganese removal from groundwater: A mechanistic and operational evaluation
Journal of Groundwater Science and Engineering. 2025, 13(4): 371-385 https://doi.org/10.26599/JGSE.2025.9280060

Transformation of ammonium nitrogen and response characteristics of nitrifying functional genes in tannery sludge contaminated soil
Journal of Groundwater Science and Engineering. 2022, 10(3): 223-232 https://doi.org/10.19637/j.cnki.2305-7068.2022.03.002

Quantitative study on vertical distribution of heat flow in Niutuozhen geothermal field, Xiong'an New Area—Evidence from heat flow determination in the Archean of D01 well
Journal of Groundwater Science and Engineering. 2025, 13(1): 22-33 https://doi.org/10.26599/JGSE.2025.9280036

Stable chlorine isotopic signatures and fractionation mechanism of groundwater in Anyang, China
Journal of Groundwater Science and Engineering. 2022, 10(4): 393-404 https://doi.org/10.19637/j.cnki.2305-7068.2022.04.007

Mechanism of seepage heat transfer in thermal reservoirs of high temperature metamorphic rocks in the Yanggao-Tianzhen basin
Journal of Groundwater Science and Engineering. 2026, 14(3): 323-341 https://doi.org/10.26599/JGSE.2026.9280085

Journal of Groundwater Science and Engineering 14(2026) 478–492

Journal homepage: http://gwse.iheg.org.cn

Research Article

Adsorption mechanism of flumequine onto kaolinite: Evidence from density functional theory calculations and the effects of Cu(II)

Yan-dan Li[1,2,+], Bing-bing Li[1,+], Dan Zhang[2], Hong-han Chen[1], Hai-jiao Xie[3], Er-ping Bi[1*]

[1] *School of Water Resources and Environment, Key Laboratory of Groundwater Conservation of MWR, and State Key Laboratory of Geomicrobiology and Environmental Changes, China University of Geosciences (Beijing), Beijing* 100083, *China*.
[2] *Beijing Key Laboratory for Risk Modeling and Remediation of Contaminated Sites, Beijing Municipal Research Institute of Eco-Environmental Protection, Beijing* 100037, *China*.
[3] *Hangzhou Yanqu Information Technology Co., Ltd, Hangzhou* 310003, *China*.

Abstract: Flumequine (FLU) is widely applied in animal husbandry and can enter sediment and groundwater systems. However, the adsorption mechanisms of FLU onto clay minerals remain unclear. Density Functional Theory (DFT) calculations were employed to elucidate the adsorption mechanism of FLU onto kaolinite, and batch adsorption experiments were conducted to investigate the adsorption behavior of FLU. Results of DFT calculations demonstrated that the carboxyl group of FLU interacted with the hydroxyl groups on the kaolinite (001) surface via hydrogen bonding and electrostatic interactions, which were the main adsorption mechanisms. The adsorption of FLU onto kaolinite exhibited pH dependence, due to pH-induced variations in both the speciation of FLU and the surface charge of kaolinite. Ionic strength negatively affected FLU adsorption because NaCl could decrease the activity of FLU, and Cl^- could also compete for the adsorption sites with FLU^-. With the addition of Cu(II), the species $Cu(FLU^-)^+$ was formed, and it had stronger adsorption affinity for kaolinite than FLU. However, Cu^{2+} could compete for adsorption sites with $Cu(FLU^-)^+$. Therefore, the molar concentration difference between $Cu(FLU^-)^+$ and Cu^{2+} played a crucial role in FLU adsorption. When the ratio of this difference in the binary systems to the adsorbed FLU in the single system exceeded 1.0, Cu(II) addition significantly enhanced FLU adsorption onto kaolinite; otherwise, it inhibited adsorption. Our findings indicate that hydrogeochemical conditions and coexisting heavy metal ions should be considered when studying the environmental fate of quinolone antibiotics.

Keywords: Flumequine; Kaolinite; Adsorption mechanism; Density functional theory; pH and ionic strength; Coexisting Cu(II)

Received: 31 Aug 2025/ Accepted: 16 Mar 2026/ Published: 10 Oct 2026

Introduction

Flumequine (FLU) is a synthetic first-generation quinolone antibiotic that has been widely used in animal feeding for treating bacterial infections (Zhao et al., 2023). Furthermore, FLU is directly added in large quantities into water as a feed additive in aquaculture (Xue et al., 2022). Due to extensive usage and its resistance to degradation, FLU has been ubiquitously detected in surface water, sediments, and groundwater at concentrations ranging from ng/L to μg/L (Zainab et al., 2021). FLU released into the environment might induce drug resistance of microorganisms and cause a potential threat to human health. The adsorption of FLU is a crucial process affecting its environmental fate and bio-accumulation. However, studies concerning the adsorption behaviors and mechanisms of FLU are relatively limited.

At present, numerous experiments have been conducted to investigate the adsorption and migra-

*Corresponding author: Er-ping Bi, *E-mail address*: bi@cugb.edu.cn

+: These authors contributed equally to this work.

DOI: 10.26599/JGSE.2026.9280090

Li YD, Li BB, Zhang D, et al. 2026. Adsorption mechanism of flumequine onto kaolinite: Evidence from density functional theory calculations and the effects of Cu(II). Journal of Groundwater Science and Engineering, 14(4): 478-492.

2305-7068/© 2026 Journal of Groundwater Science and Engineering Editorial Office This is an open access article under the CC BY-NC-ND license (http://creativecommons.org/licenses/by-nc-nd/4.0)

tion patterns of antibiotics onto soils (Wang et al., 2023; Xu et al., 2021b), clay minerals (Ortiz-Ramos et al., 2022) and humic acids (Hu et al., 2025). The results of these studies indicate that antibiotics can be adsorbed onto various adsorbents through electrostatic attraction, hydrogen bonding, hydrophobic interaction, cation exchange and surface complexation (Haciosmanoglu et al., 2022; Zhao et al., 2023). The adsorption behaviors of antibiotics are influenced by temperature, solution pH, ionic strength, the co-existence of heavy metals, dissolved organic matter, and so on (Alvarez-Esmorís et al., 2021). The solution pH is a significant parameter affecting adsorption due to the pH-dependent speciation of antibiotics and charge characteristics of soils/mineral surfaces (Maged et al., 2020). Ionic strength can indirectly promote the adsorption of antibiotics through salting out effects (Haciosmanoglu et al., 2022), while it can inhibit adsorption by competing with antibiotics for adsorption sites (Wang et al., 2025), and reducing the activity of antibiotics (Gao and Pedersen, 2005). In addition, in soil and groundwater systems, antibiotics often coexist with heavy metals (e.g., Cu(II), Cd(II), Zn(II)). It has been shown that heavy metals can enhance the adsorption of antibiotics through surface bridging (Ke et al., 2023) and complexation (Wang et al., 2023). For example, Cd(II) can enhance the adsorption of sulfamethazine onto activated carbon due to the formation of a sulfamethazine-Cd(II) ternary surface complex (Xu et al., 2021a). Meanwhile, Xu et al. (2021b) found that Cu(II) inhibits the adsorption of sulfadiazine onto paddy soil by inducing the precipitation of soil minerals. Yu et al. (2020) reported that in the binary system, Cd(II) and Pb(II) can reduce the adsorption of levofloxacin by competing for adsorption sites. However, there is a lack of research on the adsorption mechanisms of FLU onto clay minerals, and insufficient investigation into the effects of different hydrogeochemical environments on FLU adsorption behaviors. Notably, in the presence of Cu(II), the influences of Cu(II) concentration on FLU adsorption onto clay minerals at different pH remain unclear.

Therefore, kaolinite was selected as a typical clay mineral to investigate its adsorption mechanisms for FLU in this study. The objectives were to: (i) investigate the adsorption behaviors of FLU onto kaolinite at different pH and ionic strengths; (ii) clarify the adsorption mechanisms of FLU onto kaolinite using density functional theory (DFT); and (iii) study the effects of Cu(II) concentration on the adsorption of FLU onto kaolinite based on the complexation of FLU and Cu(II). The findings can be helpful for understanding the transport of FLU in environments.

1 Materials and methods

1.1 Materials

The kaolinite (chemical reagent grade) was obtained from Tianjin Fuchen Chemical Reagents Factory, China, and was used without further purification. The cation exchange capacity (13.0 mmol/kg) of kaolinite was determined at pH 7.0 by the NH_4OA_C method (Borden and Giese, 2001). The N_2-BET specific surface area (Micromeritics ASAP 2046, Norcross, Georgia, USA) of the kaolinite is 64.5 m^2/g. FLU (98% purity) was purchased from J&K Beijing, China. The structure and physicochemical properties of FLU are shown in Table S1. Anhydrous cupric chloride ($CuCl_2$, purity 99%) as well as other chemicals such as NaCl, NaOH, HCl, KH_2PO_4, and H_3PO_4 were obtained from Sinopharm Chemical Reagent Beijing, China. Methanol was HPLC grade, and Milli-Q water was used throughout the experiments.

1.2 Adsorption and desorption experiments

The solubility of FLU varies with pH; a higher pH value results in higher solubility (Khandal et al., 1991). In our research, FLU (100 mg/L) was dissolved in solution with 0.001 M NaOH as a stock solution, which was stored at 4°C and used within a week. Both adsorption and desorption experiments were conducted in triplicate using the standard batch equilibration method. All the experiments were carried out in 20-mL brown glass centrifuge tubes with Teflon-lined screw caps. For each sample, 0.10 g of kaolinite was dispersed in 20 mL FLU solution and mixed on a reciprocal shaker at 175 rpm at 25°C in the dark to avoid photolysis. The background solution was 0.01 M NaCl unless otherwise stated.

The concentration of FLU detected in the groundwater of urban-rural areas ranged from 0.01 ng/L to 4.85 ng/L (Zainab et al., 2021), while the concentration of Cu(II) detected in groundwater of the same region was in the range of 0–6.28 mg/L (Khalid et al., 2020). Clearly, the concentration of Cu(II) in groundwater is higher than that of FLU. To simulate the co-existence scenario in real environments, several molar concentration ratios of FLU to Cu(II) (1.3:1, 1:1.5, 1:3, and 1:10) were selected.

The experiments on kinetics of FLU (0.065 mM) adsorption onto kaolinite with and without 0.05/0.20 mM Cu(II) at initial pH 6.0 ± 0.1 were conducted. The samples were taken from the shaker at time intervals of 0.5, 1.0, 2.0, 4.0, 6.0, 16.0, 24.0, and 48.0 h. After the experiments, the concentrations of FLU and Cu(II) in the supernatant were analyzed, and the final pH was measured. The FLU (0.014 mM to 0.07 mM) experiments with/without 0.10 mM Cu(II) for adsorption isotherms were performed at initial pH 6.0 ± 0.1 and 9.0 ± 0.1, respectively.

The effects of pH and ionic strength on the adsorption of FLU onto kaolinite were investigated through batch adsorption edge experiments conducted in 0.001, 0.01, and 0.10 M NaCl solutions, respectively. The initial concentration of FLU was 0.07 mM. The initial pH ranged from 4.0 to 11.0. The effects of Cu(II) on FLU adsorption onto kaolinite at different pH values were investigated. In brief, initial pH values (4.0–11.0) of 0.07 mM FLU solutions with/without 0.05, 0.10, and 0.20 mM Cu(II) were adjusted by 0.10 M HCl and NaOH. For desorption experiments, the supernatant at pH 7.0 ± 0.1 was removed after the isothermal adsorption experiments, and the volume was measured by the weighing method. Subsequently, 20 mL of 0.01 M NaCl solution with/without Cu(II) was added. Then, the tubes were resealed and agitated for 48 h, and three sequential desorption steps were performed. After each experiment was completed, the FLU concentration in the supernatant was analyzed and the final pH was measured immediately.

1.3 Analytical methods

FLU was analyzed by high performance liquid chromatography (HPLC, Shimadzu Corp, LC-20AT, Japan) equipped with an InterSustainSwift C18 column (5 μm, 4.6 mm × 250 mm). The UV detector wavelength was set at 248 nm, and the mobile phases were 60:40 (v:v) of methanol and Milli-Q water with 0.1% H_3PO_4; the flow rate was 0.8 mL/min. The column was kept at 30 °C and the injection volume was 10 μL.

1.4 Data analysis

The amount of FLU adsorbed onto kaolinite was calculated by Eq. (1).

$$q_t = \frac{(C_0 - C_t)v}{m} \tag{1}$$

Where: C_0 (mM) is the initial concentration of FLU, C_t (mM) is the aqueous concentration of FLU at time t, and q_t (mmol/kg) is the amount of FLU adsorbed onto kaolinite at time t.

The adsorption kinetic data of FLU were described by the Pseudo-First-Order kinetic Model (PFOM) (Eq. 2) and the Pseudo-Second-Order kinetic Model (PSOM) (Eq. 3).

$$q_t = q_e(1 - e^{-k_1 t}) \tag{2}$$

$$q_t = \frac{k_2 q_e^2 t}{1 + k_2 q_e t} \tag{3}$$

Where: q_e (mmol/kg) is the equilibrium adsorption capacity of FLU, k_1 (h^{-1}) and k_2 [kg/(mmol·h)] are the rate constants of PFOM and PSOM, respectively.

The linear (Eq. 4), Freundlich (Eq. 5) and Langmuir (Eq. 6) models were used to fit equilibrium adsorption data.

$$q_e = K_d C_e \tag{4}$$

$$\ln q_e = \ln K_F + n \ln C_e \tag{5}$$

$$q_e = \frac{K_L q_m C_e}{1 + K_L C_e} \tag{6}$$

Where: K_d (L/kg) is the distribution coefficient of the solid/liquid ratio, K_F ([(mmol/kg)/$(mM)^n$]) and n are the constants that give estimates of the adsorptive capacity and intensity, q_m (mmol/kg) represents the maximum adsorption capacity and K_L (L/mmol) is the Langmuir equilibrium constant, and C_e (mM) is the mass concentration of FLU in the liquid phase.

1.5 DFT calculation

The (001) crystal plane is the most easily cleaved and major cleavage plane of kaolinite (Han et al., 2016). Cleavage of kaolinite crystals along the (001) plane exposes siloxane and aluminol hydroxyl surfaces (Han et al., 2016). Previous studies have shown that the aluminol hydroxyl surface is more polar, richer in hydroxyl functional groups, and exhibits significantly stronger adsorption capacity for pollutants than the siloxane surface (Zhao et al., 2022). Therefore, the aluminol hydroxyl surface of kaolinite (001) was selected as the research object for molecular simulations in this study, hereinafter referred to as the kaolinite (001) surface. The Density Functional Theory (DFT) calculations were carried out with the VASP code (Pantaleone et al., 2020). The Perdew–Burke–Ernzerhof (PBE) functional within the Generalized Gradient Approximation (GGA) was used to process the exchange–correlation, while the Projector Augmented-Wave pseudopo-

tential (PAW) was applied with a kinetic energy cut-off of 500 eV, and utilized to describe the expansion of the electronic eigenfunctions. The periodic supercell (2 × 2 × 1) slab with a vacuum thickness of 15 Å was used to describe the kaolinite (001) surface to minimize interlayer interactions (Fig. S1). The Brillouin-zone integration was sampled by a Γ-centered 3 × 3 × 1 Monkhorst–Pack k-point. All atomic positions were fully relaxed until energy and force reached tolerances of 1×10^{-5} eV and 0.02 eV/Å, respectively. The dispersion-corrected DFT-D3 method was employed to consider the long-range interactions (Deogratias et al., 2023).

In order to study the adsorption of FLU onto the kaolinite (001) surface, three possible adsorption configurations were considered, namely the carbonyl group, carboxyl group, and F group of FLU oriented towards the kaolinite (001) surface. In the following text, they are denoted as KAO-CO, KAO-COOH, and KAO-F adsorption configurations, respectively. These configurations were geometry-optimized, following which the adsorption energy (E_{ads}) and the charge density difference were calculated by Eq. (7) and Eq. (8).

$$E_{\text{ads}} = E_{total} - (E_{surface} + E_{FLU}) \quad (7)$$

$$\Delta\rho = \rho_{\text{total}} - (\rho_{surface} + \rho_{FLU}) \quad (8)$$

Where: E_{total}, $E_{surface}$ and E_{FLU} are the energies of the whole adsorption configuration, the kaolinite (001) surface, and the FLU molecule, respectively; and ρ_{total}, $\rho_{surface}$ and ρ_{FLU} are the charge densities of the whole adsorption configuration, the kaolinite (001) surface, and the FLU molecule, respectively.

2 Results and discussion

2.1 Adsorption kinetics

The FLU adsorption onto kaolinite (Fig. 1a) could be divided into two stages, namely the initial rapid adsorption stage and the later slow adsorption equilibrium stage. Within the first 6 h, because there were a large number of adsorption sites on the surface of kaolinite, FLU was easily adsorbed onto kaolinite. The adsorption quantity accounted for approximately 80.8% of the total equilibrium capacity at the first 6 h. As the experiments continued, the adsorption sites gradually reached saturation, causing the adsorption rate to slow down, and finally reach equilibrium at 48 h. The PFOM and PSOM were used to fit the adsorption kinetic data of FLU onto kaolinite (Table S2), with the PSOM providing a better fit to the experimental data.

The presence of Cu(II) significantly influenced the FLU adsorption equilibrium time and adsorption capacity. In the FLU and Cu(II) binary system, FLU reached adsorption equilibrium at about 10 h. At the same time, the equilibrium adsorption capacity also changed. The total adsorbed FLU (FLU and FLU-Cu(II) complexes) increased with the addition of 0.05 mM Cu(II), but decreased with the addition of 0.20 mM Cu(II). After 24 h, the adsorption amount of FLU was 3.73 mmol/kg. However, when 0.05 mM and 0.20 mM Cu(II) were added, the adsorption amounts were 5.51 mmol/kg and 3.07 mmol/kg, respectively. The reason was that excessive Cu(II) (i.e., 0.20 mM) would compete for adsorption sites with FLU-Cu(II) complexes. This phenomenon is similar to the coexistence of ofloxacin and Cu(II) adsorption

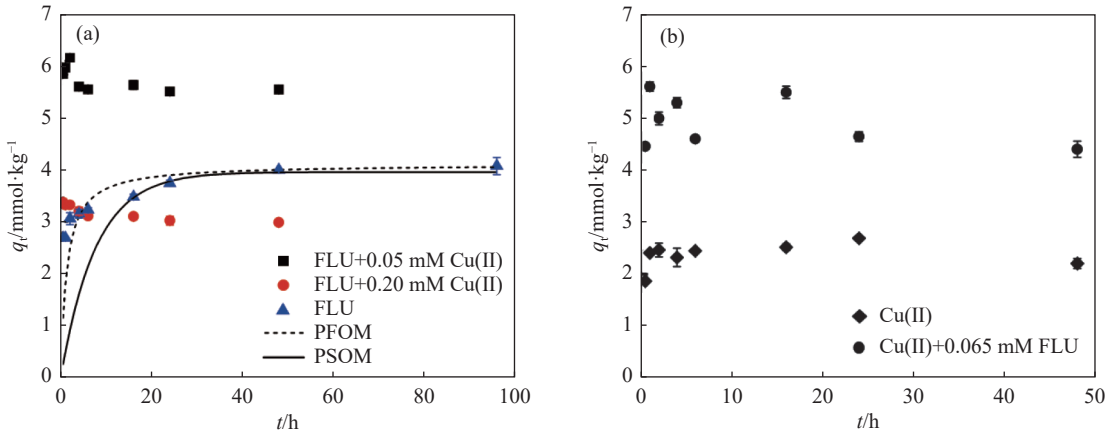


Fig. 1 The adsorption kinetics of FLU and Cu(II) onto kaolinite (final solution pH 5.4 ± 0.1) (a) FLU (0.065 mM) with/without 0.05 and 0.20 mM Cu(II); (b) Cu(II) (initial concentration 0.20 mM) with/without 0.065 mM FLU

onto kaolinite (Li et al., 2017) and the coexistence of ciprofloxacin and Cu(II) adsorption onto graphene hydrogels (Ma et al., 2020), indicating that the antibiotic adsorption capacity is closely related to the concentration of Cu(II).

Cu(II) addition significantly changed the shape of the kinetics curve of FLU adsorption (Fig. 1a). When FLU coexisted with Cu(II), the amount of FLU adsorbed onto kaolinite decreased within the first 8 h, which might be due to desorption (Guaita et al., 2011), and then FLU reached adsorption equilibrium at 10 h. Therefore, neither the PFOM nor the PSOM was applicable to the adsorption kinetic data of the FLU and Cu(II) binary system. Furthermore, FLU also promoted the adsorption of Cu(II) onto kaolinite (Fig. 1b). After 48 h, the Cu(II) adsorption amount increased from 2.21 mmol/kg to 4.96 mmol/kg, suggesting that the affinity of FLU-Cu(II) complexes for kaolinite was stronger than that of Cu(II) ions.

2.2 Adsorption isotherms

The dissociation constant (pK_a) of FLU is 6.35. At pH 5.4, FLU primarily exists in the form of FLU^0, and at pH 7.8 it primarily exists as FLU^-. Adsorption isotherm experiments of the FLU single system and the FLU and Cu(II) binary system were conducted with the final solution pH of 5.4 ± 0.1 and 7.8 ± 0.1.

When FLU acted as the adsorbate, the linear model provided the best fit under both pH conditions (Fig. 2, Table 1). The K_d values of FLU adsorbed onto kaolinite at pH 5.4 ± 0.1 and 7.8 ± 0.1 were 105.19 L/kg and 6.23 L/kg, respectively. The decreased adsorption resulted from the electrostatic repulsion that occurred between FLU^- and the negatively charged kaolinite surface at pH 7.8 ± 0.1. When FLU (0.014–0.07 mM) coexisted with 0.10 mM Cu(II), all three isotherm models exhibited excellent fitting results. At pH 5.4 ± 0.1, the participation of Cu(II) inhibited the adsorption of FLU onto kaolinite (Fig. 2a), and the K_d value decreased from 105.19 L/kg to 63.79 L/kg due to excessive Cu(II) competing for adsorption sites. At pH 7.8 ± 0.1, Cu(II) instead promoted the adsorption of FLU (Fig. 2b), and the K_d value increased from 6.23 L/kg to 144.66 L/kg since excessive Cu(II) existed as $Cu(OH)_2$ and did not compete for adsorption sites with FLU-Cu(II) complexes. This is similar to the phenomenon that tetracycline could tightly bind with adsorbents through complexation with Cu(II), greatly enhancing its adsorption (Xiong et al., 2024).

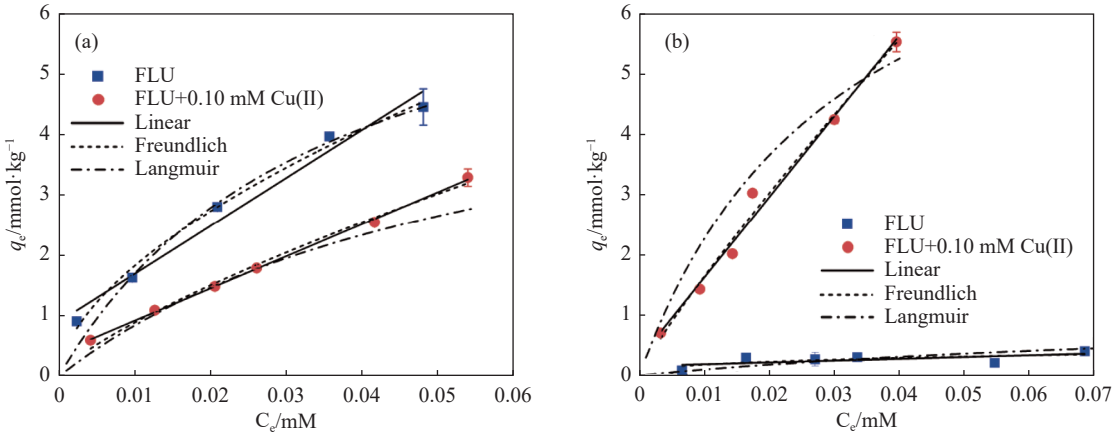


Fig. 2 Adsorption isotherm fitting curves of FLU with/without 0.10 mM Cu(II) under different final pH conditions ((a) pH 5.4 ± 0.1; (b) pH 7.8 ± 0.1)

Table 1 Fitting parameters of isotherm models of FLU with/without 0.10 mM Cu(II)

pH	Adsorbates	Linear		Freundlich			Langmuir		
		K_d (1)	R^2	K_F (2)	n	R^2	q_m	K_L (3)	R^2
5.4	FLU	105.19	0.97	23.16	0.54	0.99	7.79	27.98	0.99
	FLU+Cu(II)	63.79	0.99	20.71	0.66	0.99	5.76	17.16	0.98
7.8	FLU	6.23	0.84	1.48	0.51	0.60	1.15	9.11	0.18
	FLU+Cu(II)	144.66	0.99	81.69	0.84	0.98	9.35	32.17	0.95

Notes: (1) the unit is L/kg; (2) the unit is $(mmol/kg)/(mM)^n$; and (3) the unit is L/mmol

2.3 Effects of pH and ionic strength

2.3.1 Effect of solution pH

The solution pH has an impact on the surface charge of minerals and the existence forms of antibiotics in solutions (Alvarez-Esmorís et al., 2021). The zeta potential of kaolinite used in this study had been measured in our previous research, which showed that the kaolinite became more negatively charged with increasing pH (Li et al., 2017). At pH < pK_a (6.35), FLU^0 is the major species. As the pH value increases, carboxyl group dissociates, and the proportion of FLU^0 gradually decreases, while the proportion of FLU^- increases. Therefore, the adsorption mechanism between FLU and kaolinite might be different under different pH conditions.

The adsorption of FLU onto kaolinite was strongly influenced by the solution pH (Fig. 3). When the solution pH was in the range of 4.0 to 6.0, the q_e increased with increasing pH. At about pH 6.0, the q_e reached a maximum of 4.10 mmol/kg in 0.01 M NaCl solution. At pH > 6.0, and the q_e decreased with increasing pH; the q_e was 0.01 mmol/kg in 0.01 M NaCl solution at pH 8.95; the adsorption of FLU was almost not observed at pH 10.0. The change in the adsorption behavior of FLU onto kaolinite with pH is the same as that of nalidixic acid, which reached the maximum adsorption amount at pH around pK_a (Cheng et al., 2023). This phenomenon is related to the species of FLU and the surface properties of kaolinite varying with pH.

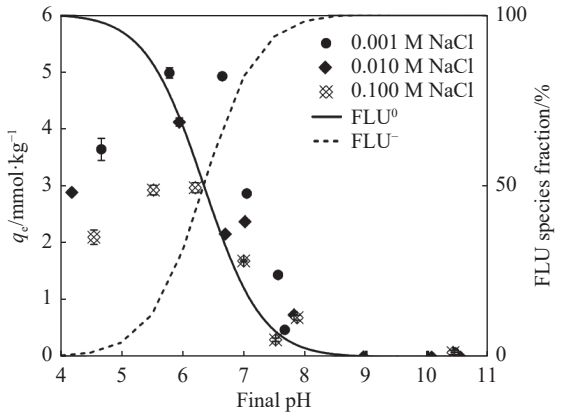


Fig. 3 The adsorption amount of FLU onto kaolinite with different NaCl concentrations

The FLU species distribution curves under different pH conditions are illustrated in Fig. 3. Previous studies showed that there were two types of adsorption sites on the kaolinite surface, including the permanent negatively charged sites on the basal siloxane surface and the variable charged sites on the edge (Nguyen et al., 2023). Nonspecific ion exchange reaction occurred on the basal siloxane surface, and surface complexation reactions occurred on the edge sites (Zhao et al., 2015). The edge of the kaolinite contained Si hydroxyl group (SiOH) and Al hydroxyl group (AlOH), the increasing dissociation of SiOH with pH led to enhanced electronegativity of the kaolinite. The pK_{a1} of the AlOH on the edge of the kaolinite was 6.30 ($AlOH+H^+ \Leftrightarrow AlOH_2^+$), and the pK_{a2} was 8.70 ($AlOH \Leftrightarrow AlO^- + H^+$). It was reported that the –COOH/–COO^- of fluoroquinolones could be adsorbed onto kaolinite by hydrogen bonding (Zhao et al., 2015).

At pH < 6.0, FLU^0 was the main species; it could be adsorbed onto kaolinite through hydrogen bonding and hydrophobic interaction, and FLU^- could also be adsorbed onto kaolinite by electrostatic attraction with the $AlOH_2^+$. At pH 6.0, the proportions of FLU^0 and FLU^- were 61.3% and 38.7%, respectively; the AlOH with a pK_{a1} of 6.30 was mainly in the forms of AlOH and $AlOH_2^+$. Consequently, the maximum q_e of FLU was observed. With increasing pH, the proportion of $AlOH_2^+$ decreased, while the proportions of SiO^-, AlO^- and FLU^- increased, causing hydrophobic interaction to weaken and electrostatic repulsion to increase. The adsorption affinity of FLU for kaolinite weakened as the solution pH increased from 6.0 to 11.0.

2.3.2 Effect of ionic strength

With increasing ionic strength, the q_e obviously decreased (Fig. 3). At pH 4.5, FLU^0 was the main species; the q_e values were 3.63, 2.88 and 2.10 mmol/kg for the ionic strengths of 0.001, 0.01 and 0.10 M, respectively. There was no competitive adsorption of Cl^- or Na^+ with FLU^0, the inhibitory effect on adsorption might be caused by the restrained activity of FLU^0 in the solution with high ionic strength. At pH 7.0, the percentages of FLU^0 and FLU^- were 13.72% and 86.31%, and the q_e values of FLU adsorption onto kaolinite were 2.86 mmol/kg, 2.37 mmol/kg and 1.68 mmol/kg at 0.001, 0.01 and 0.10 M NaCl, respectively. The adsorption ability of FLU^- onto kaolinite was suppressed since the high concentration of NaCl weakened the activity of FLU and the increasing Cl^- also competed for adsorption sites with FLU^-. At pH > 7.0, the inhibitory effect of ionic strength on the adsorption of FLU was weakened. This is because the current acid-base condition of the solution led to a decrease in the dissociated $AlOH_2^+$ on the kaolinite, and an increase in AlO^-, making the

competitive adsorption of Cl^- diminish. In consequence, with increasing ionic strength, the adsorption of FLU onto kaolinite decreased. This result is different from the adsorption of ciprofloxacin, in which ionic strength promoted the adsorption of ciprofloxacin onto goethite. This phenomenon can be explained by Cl^- shielding the surface charge and compressing the electrical double layer (Luo et al., 2024).

The effect of ionic strength on the adsorption of organic pollutants was also used to provide information on surface complexation. A restraining effect of ionic strength on adsorption indicated an outer-sphere surface complexation mechanism (Chassé et al., 2015). The adsorption amount of FLU decreased with increasing ionic strength in the final pH range of 4.2 to 10.5, which indicated that the complexation of $-COO^-$ with kaolinite was not the main mechanism, but rather the electrostatic attraction of FLU^- was the main adsorption mechanism to kaolinite.

2.4 DFT analysis of adsorption mechanisms

DFT calculations were used to verify the mechanisms of FLU adsorption onto kaolinite at the molecular level. The three optimized adsorption configurations are shown in Fig. 4, and the bonding atoms and bond lengths in each configuration are summarized in Table S3. In the KAO-CO configuration, the carbonyl group of FLU formed a hydrogen bond with the surface hydroxyl groups, with a bond length of 1.83 Å. Under this condition, since the carboxyl group of FLU was close to the carbonyl group, the carboxyl group was also exposed to the surface hydroxyl groups, forming another hydrogen bond with a bond length of 1.88 Å (Fig. 4a). In the KAO-COOH configuration, the carboxyl group of FLU could form three hydrogen bonds with the surface hydroxyl groups, with bond lengths of 1.75 Å, 1.96 Å, and 1.98 Å, respectively. Additionally, the carbonyl group also formed a hydrogen bond with the surface hydroxyl groups (Fig. 4b). In the KAO-F configuration, the F group of FLU was far from the hydroxyl groups of the kaolinite (001) surface, and thus no hydrogen bonds were formed (Fig. 4c). Generally speaking, the shorter the bond length, the stronger the bonding strength (Zhang et al., 2021). In addition, the Crystal Orbital Hamiltonian Population (COHP) was also a powerful tool for measuring bonding strength. The integral of COHP from the lowest energy state to the Fermi level was defined as *ICOHP*. The more negative the *ICOHP* value, the stronger the bonding interaction between atomic pairs, and the greater the contribution to the stability of the system (George et al., 2022). The graphs of the variation of COHP with energy of each hydrogen bond formed in the three adsorption configurations, as well as the *ICOHP* values, are provided in the Supplementary Materials (Figs. S2-S4, Table S3). The number of atoms mentioned here were all derived from the POSCAR input file. For the KAO-F adsorption configuration, the closest H_{11}…F atomic pair was selected for analysis.

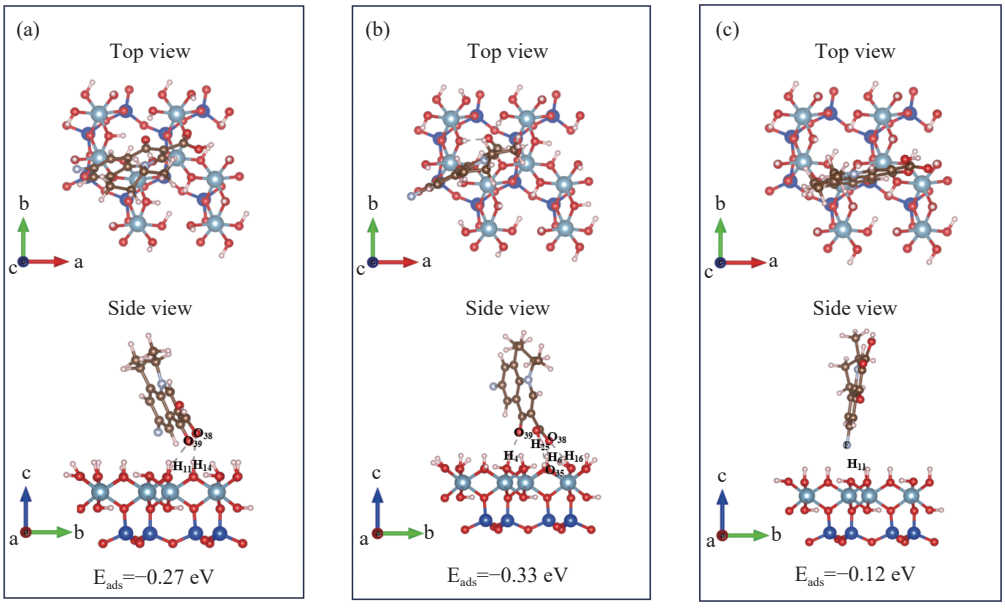


Fig. 4 Three optimized configurations of FLU adsorption onto kaolinite (001) surface

Notes: (a): KAO-CO; (b): KAO-COOH; (c): KAO-F

It was found that the *ICOHP* value of the hydrogen bond between the carboxyl O_{38} atom of FLU and the hydroxyl H_{16} atom on the kaolinite surface was the smallest, indicating that the hydrogen bond interaction between the carboxyl group of FLU and the hydroxyl group of kaolinite was the strongest.

Apart from hydrogen bonding, there were also electrostatic interactions between FLU and the kaolinite (001) surface (Fig. 5). The charge accumulation and depletion were represented by yellow and light blue, respectively. In the interaction region between FLU and the kaolinite (001) surface, the charge densities of surface H atoms decreased (charge depletion), while the charge densities of O and F atoms of FLU increased (charge accumulation). In other words, from a local perspective, charge was transferred from the H atoms on the kaolinite surface to the O and F atoms of FLU, which reflected the bonding interactions between specific atoms (Zhao et al., 2025). By calculating the gain and loss of Bader charge for each atom in the adsorption configurations, the direction and magnitude of charge transfer could be understood from a holistic perspective. A positive change of Bader charge indicated that the atom had gained electrons, while a negative change indicated that it had lost electrons (Table 2). It was found that charge was transferred from FLU to the kaolinite surface in all three adsorption configurations, among which the KAO-COOH configuration exhibited the largest charge transfer amount, which was 0.033 e. This seemingly contradictory phenomenon might be related to the fact that local charge transfer can induce charge redistribution within the kaolinite surface and FLU (Zhao et al., 2025).

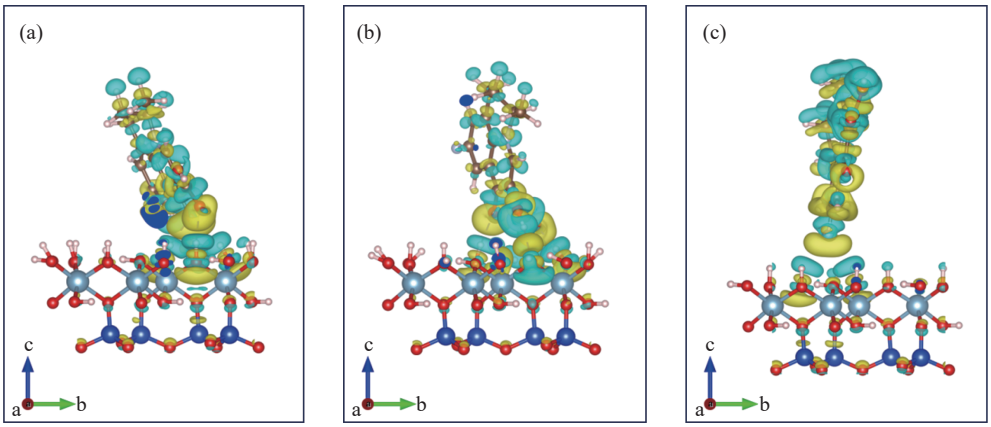


Fig. 5 The charge density difference diagrams of three adsorption configurations

Notes: (a): KAO-CO; (b): KAO-COOH; (c): KAO-F

Table 2 The average Bader charge and the amount of charge change of each atom in the three adsorption configurations

Items	*Charge*			*△Charge*		
	KAO-CO	KAO-COOH	KAO-F	KAO-CO	KAO-COOH	KAO-F
$Al^{(1)}$	0.511	0.512	0.511	−2.489	−2.488	−2.489
$Si^{(1)}$	0.816	0.816	0.816	−3.184	−3.184	−3.184
$O^{(1)}$	7.531	7.534	7.527	1.531	1.534	1.527
$H^{(1)}$	0.392	0.385	0.400	−0.608	−0.615	−0.600
$C^{(2)}$	3.726	3.721	3.730	−0.277	−0.278	−0.270
$N^{(2)}$	6.200	6.190	6.190	1.200	1.190	1.190
$F^{(2)}$	7.640	7.630	7.670	0.640	0.630	0.670
$O^{(2)}$	7.138	7.149	7.119	1.138	1.149	1.119
$H^{(2)}$	0.879	0.883	0.880	−0.121	−0.117	−0.120
$Q^{(3)}$	–	–	–	0.031	0.033	0.002

Notes: (1) the atoms of the kaolinite (001) surface; (2) the atoms of FLU; and (3) the amounts of charge transfer of the three configurations (positive Q indicated that charge was transferred from FLU to the kaolinite surface)

The E_{ads} of the three adsorption configurations were −0.27 eV, −0.33 eV, and −0.12 eV, respectively. When the E_{ads} value is negative, it means that kaolinite can spontaneously adsorb FLU, and the more negative the E_{ads}, the stronger the adsorption effect. Therefore, the carboxyl group of FLU played an important role in the adsorption onto kaolinite, and hydrogen bonding and electrostatic interaction were the main mechanisms.

2.5 Effect of coexisting Cu(II) on FLU adsorption

It was reported that complexes could form between Cu(II) and FLU in aqueous solution (Urbaniak and Kokot, 2009). The species and concentration of coordination compounds varied with pH, so that the effects of co-existing Cu(II) on FLU adsorption at different pH were investigated. The speciation of FLU (0.07 mM) with Cu(II) (0.05, 0.10 and 0.20 mM, respectively) in solution as a function of pH was calculated (Fig. 6).

In the binary system, the main species were FLU^0, FLU^-, free Cu(II) (i.e., Cu^{2+}), $Cu(OH)_2$, $Cu_2(OH)_2^{2+}$, $Cu(FLU^-)^+$ and $Cu(FLU^-)_2^0$. The concentrations of other hydrated cations of Cu(II) were very low and thus not shown. At a pH range of 3.0 to 7.0, when 0.05 mM Cu(II) was added, the main complexes of FLU were $Cu(FLU^-)^+$ and $Cu(FLU^-)_2^0$; when 0.10 or 0.20 mM Cu(II) was added, the main complex of FLU was $Cu(FLU^-)^+$. The residual Cu(II) existed as Cu^{2+}. At a pH range of 7.0 to 11.0, $Cu(FLU^-)_2^0$ increased with increasing pH, and $Cu(FLU^-)_2^0$, $Cu(OH)_2$ and $Cu_2(OH)_2^{2+}$ were the main species of Cu(II).

The effects of different concentrations of Cu(II) on FLU adsorption onto kaolinite are shown in Fig. 7(a). Same as ofloxacin, the effect of Cu(II) was related to the solution pH and the concentration of Cu(II) (Li et al., 2017). At pH < 7.0, when 0.07 mM FLU co-existed with 0.05 mM Cu(II), the adsorption amount of FLU increased. Under this

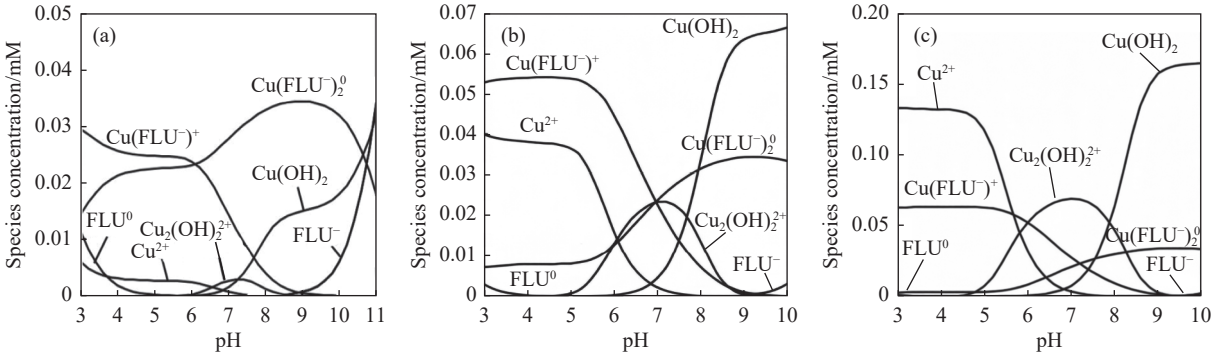


Fig. 6 Solution species of 0.07 mM FLU with (a) 0.05 mM Cu(II); (b) 0.10 mM Cu(II) and (c) 0.20 mM Cu(II) at different pH values calculated by the software ChemEQL

Notes: The stability constants were obtained from reference (Urbaniak and Kokot, 2009): $Cu^{2+} + FLU^- \Leftrightarrow Cu(FLU^-)^+$, $\log\beta = 6.00$; $Cu^{2+} + 2\,FLU^- \Leftrightarrow Cu(FLU^-)_2^0$, $\log\beta = 11.00$; $FLU^- + H^+ \Leftrightarrow FLU^0$, $pK_a = 6.35$

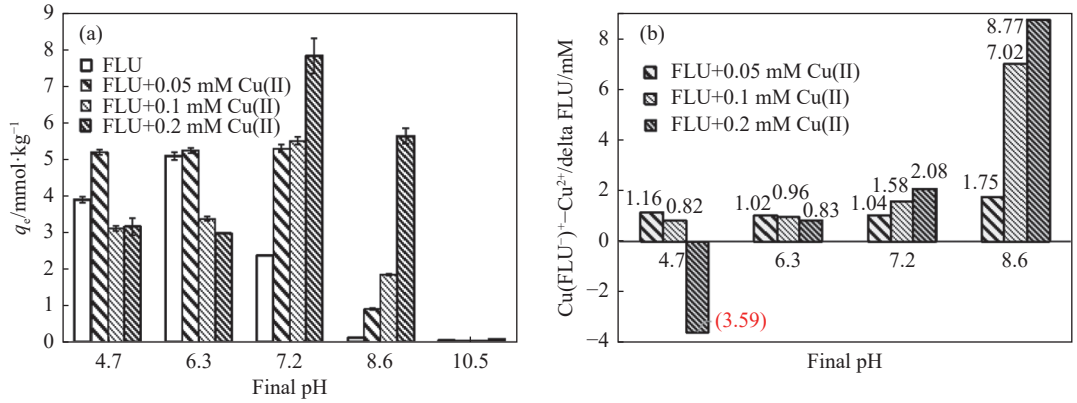


Fig. 7 (a) Adsorption of FLU (0.07 mM) with/without 0.05, 0.10, and 0.20 mM Cu(II) as a function of pH (25 °C, equilibration time 48 h, background electrolyte 0.01 M NaCl); (b) the molar concentration ratios of the difference between $Cu(FLU^-)^+$ and Cu^{2+} in the binary systems (i.e., FLU and Cu(II)) to the adsorbed FLU in the single system (i.e., FLU only) as a function of pH

condition, most of the Cu(II) was complexed, and the main species of FLU were $Cu(FLU^-)^+$ and $Cu(FLU^-)_2^0$. $Cu(FLU^-)^+$ was positively charged and could be adsorbed onto kaolinite through electrostatic attraction. In addition, it was reported that the FLU-Cu(II) complexes could promote antibiotic adsorption via forming a ternary surface complex (Guaita et al., 2011) or a bridging effect (Ma et al., 2020). These reasons might lead to an increase of the FLU adsorption onto kaolinite. However, when 0.10 mM or 0.20 mM Cu(II) was added, the increased Cu^{2+} could compete with $Cu(FLU^-)^+$ for adsorption sites, and thus decreased the adsorption amount of FLU.

The influence of co-existing Cu(II) on FLU adsorption at pH > 7.0 was different from that at pH < 7.0. At pH > 7.0, excessive Cu(II) did not entirely involve in the complexation reaction but existed in the form of $Cu(OH)_2$, which would not compete for adsorption sites. Cu(II) significantly promoted the adsorption of FLU onto kaolinite, and the promoting effect became stronger with increasing Cu(II) concentration, which proved that the affinity of $Cu(FLU^-)^+$ was higher than that of FLU^- itself. As solution pH increased, the proportion of $Cu(FLU^-)^+$ decreased, while the proportion of Cu $(FLU^-)_2^0$ increased, and the promoting effect of Cu(II) on the adsorption of FLU onto kaolinite decreased. At pH 10.5, the main species of FLU were $Cu(FLU^-)_2^0$ and FLU^-. FLU^- was not adsorbed onto kaolinite due to the electrostatic repulsion; there was no adsorption of FLU onto kaolinite, which meant that the adsorption affinity of $Cu(FLU^-)_2^0$ for kaolinite was weak.

In the binary system, $Cu(FLU^-)^+$ played an important role in the adsorption of FLU onto kaolinite. However, Cu^{2+} could compete with $Cu(FLU^-)^+$ for adsorption sites, and thus the molar concentration difference between $Cu(FLU^-)^+$ and Cu^{2+} dominated FLU adsorption. Under different experimental pH conditions, the molar concentration ratios of the difference between $Cu(FLU^-)^+$ and Cu^{2+} in the binary systems to the adsorbed FLU in the single system are illustrated in Fig. 7b. The ratio greater than 1.0 indicated that the presence of Cu(II) promoted FLU adsorption onto kaolinite; otherwise, it inhibited adsorption. When the ratio equaled 1.0, the effect of Cu(II) on FLU adsorption was negligible. This quantitative result provided a theoretical basis for predicting and assessing the environmental fate of antibiotics in heavy metal co-contaminated sites.

2.6 Desorption of FLU from kaolinite

In our experiments, the effect of Cu(II) on FLU desorption from kaolinite was investigated at different FLU adsorption amounts (Fig. 8). The desorption rates of FLU increased with increasing adsorption amounts when desorbed with a 0.01 M NaCl solution. It has been reported that organic pollutants would undergo adsorption to high-energy sites when the levels of total adsorption were low; therefore, desorption was difficult (Xu et al., 2015). These findings could explain why FLU desorption rates increased with increasing adsorption amounts. The desorption percentages of FLU in 0.01 M NaCl were in the range of 44.6% to 64.4%. The desorption rates of FLU increased to 83.6% to 95.0% in the presence of Cu(II). This was attributed to the strong complexation of Cu(II) with the adsorbed FLU, which facilitated its release (Eq. 9). Although kaolinite exhibited a higher affinity for $Cu(FLU^-)^+$ than Cu^{2+}, Cu^{2+} in the desorption solution competed for adsorption sites, thereby preventing the re-adsorption of $Cu(FLU^-)^+$. This is consistent with the conclusions from the adsorption experiments.

$$\text{Kaolinite} - \text{FLU} + \text{Cu(II)} \Leftrightarrow \text{Kaolinite} + \text{FLU} - \text{Cu(II)} \quad (9)$$

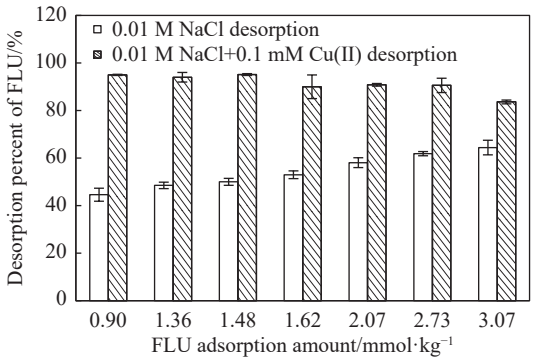


Fig. 8 Desorption of FLU in the absence/presence of Cu(II) (0.10 mM) in solution with a final pH 6.4 ± 0.1

3 Conclusion

DFT calculation results demonstrated that the carboxyl group of FLU was more likely to interact with the hydroxyl groups on the kaolinite, with the adsorption process dominated by hydrogen bonding and electrostatic interaction. The adsorption of FLU onto kaolinite was pH-dependent. Ionic strength exerted a negative effect on FLU adsorption, as NaCl reduced the activity of FLU and Cl^- competed for adsorption sites with FLU^-. Solution pH and Cu(II) concentration affected the species of FLU and Cu(II). $Cu(FLU^-)^+$ had a higher adsorption affinity than Cu^{2+} onto kaolinite. The molar

concentration difference between $Cu(FLU^{-})^{+}$ and Cu^{2+} dominated the FLU adsorption. When the ratios of this difference in the binary systems to the adsorbed FLU in the single system were greater than 1.0, Cu(II) addition significantly promoted FLU adsorption; otherwise, it inhibited adsorption. At a ratio of 1.0, the effect of Cu(II) on FLU adsorption could be neglected. Cu(II) complexed with adsorbed FLU to form $Cu(FLU^{-})^{+}$, while Cu^{2+} inhibited the re-adsorption of $Cu(FLU^{-})^{+}$, thereby promoting FLU desorption. These findings are helpful for the accurate assessment of environmental risks posed by quinolone antibiotics in heavy metal co-contaminated groundwater systems.

Supporting Information

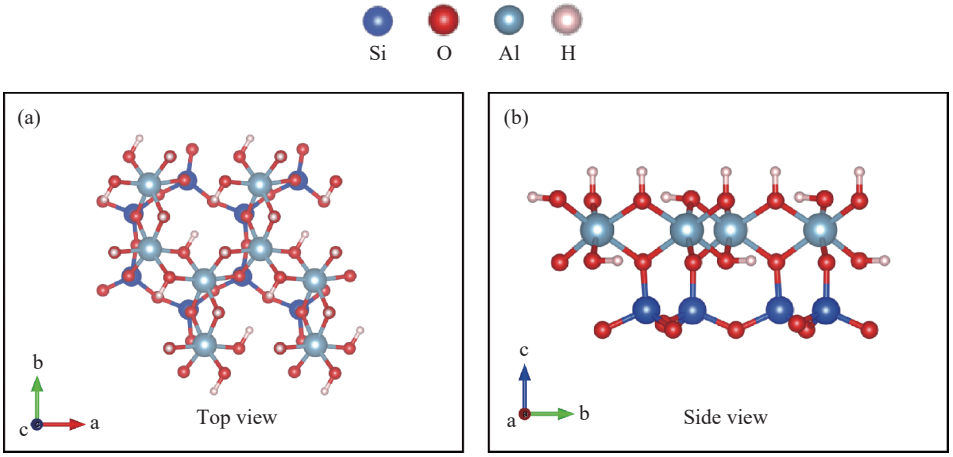


Fig. S1 The optimized structure of kaolinite (001) surface (a) Top view; and (b) Side view

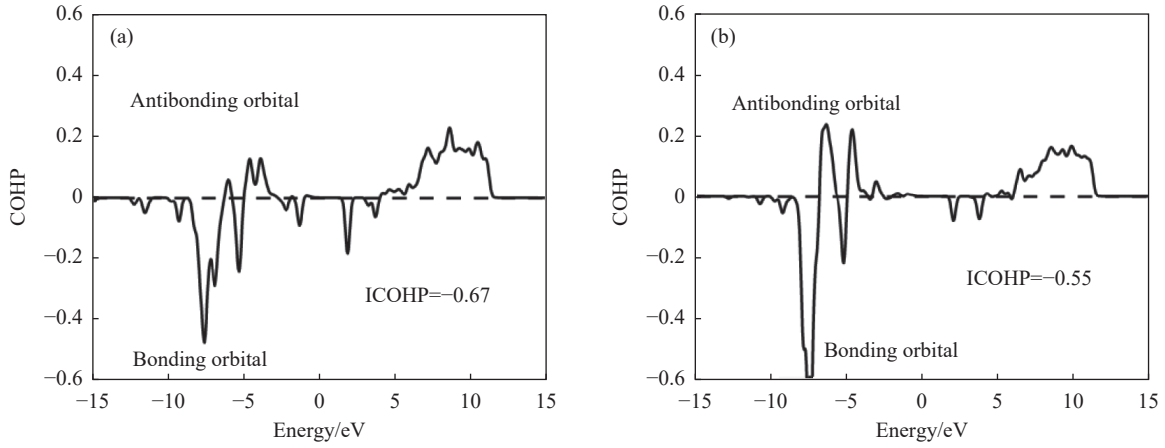
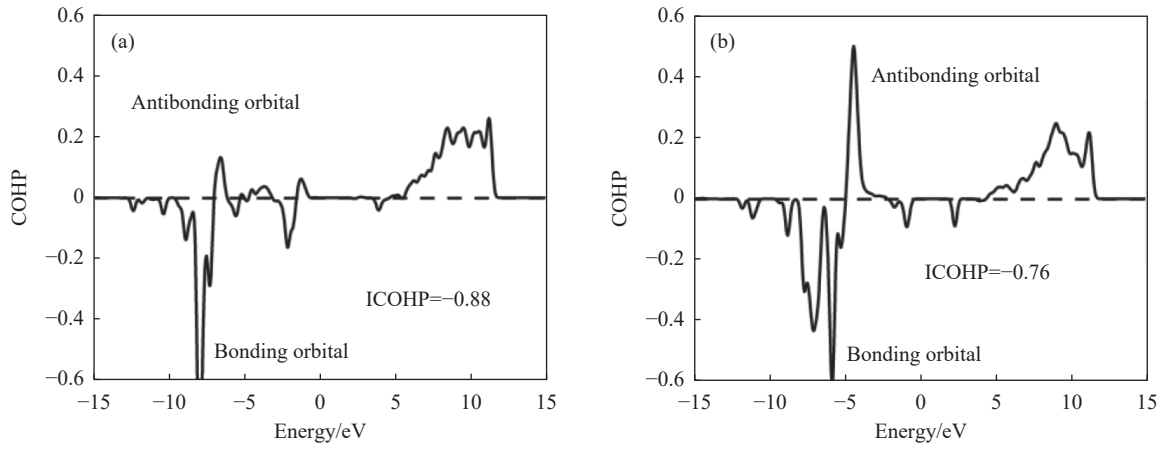


Fig. S2 The variation of COHP with energy for the bonds in the KAO-CO adsorption configuration (a) the H_{11}…O_{39} bond; and (b) the H_{14}…O_{38} bond



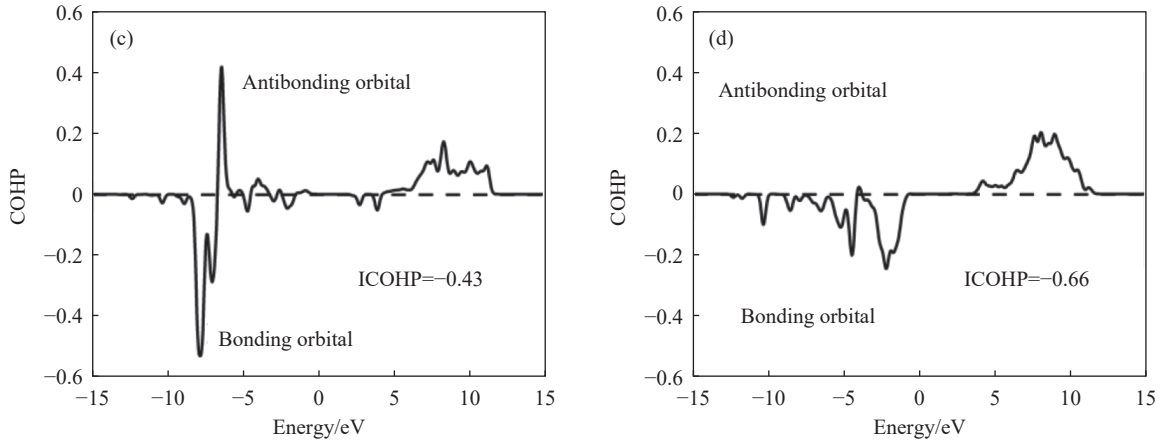


Fig. S3 The variation of COHP with energy for the bonds in the KAO-COOH adsorption configuration (a) the $H_{16}…O_{38}$ bond; (b) the $H_4…O_{39}$ bond; (c) the $H_6…O_{38}$ bond; and (d) the $O_{34}…H_{25}$ bond

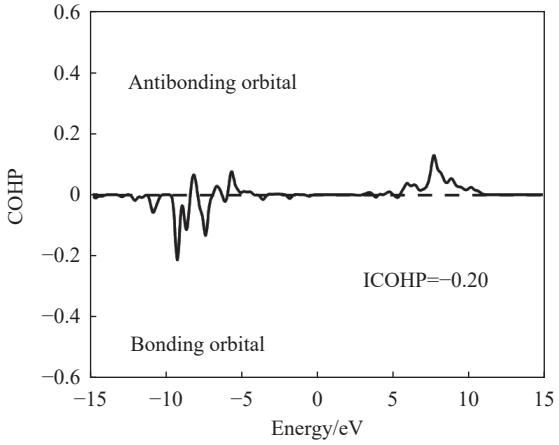
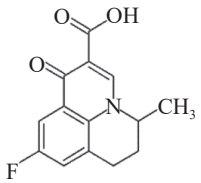


Fig. S4 The variation of COHP with energy for the $H_{11}…F$ bond in the KAO-F adsorption configuration

Table S1 Main physicochemical properties of FLU

Compound	Molecular Weight (g/mol)	pK_a	Log K_{ow}	Structure
FLU	261.25	6.35(1)	1.72(2)	

Note: (1) (Feng et al., 2016); and (2) (Van Doorslaer et al., 2014)

Table S2 Parameters of PFOM and PSOM

Adsorbates	q_e(1)	PFOM			PSOM		
		k_1(2)	q_{e1}(1)	R^2	k_2(3)	q_{e2}(1)	R^2
FLU	4.00	0.13	3.95	0.93	0.19	4.04	0.99

Note: (1) the unit is mmol/kg; (2) the unit is h^{-1}; and (3) the unit is kg/(mmol·h)

Table S3 Bonding analysis of the three adsorption configurations

configurations	Bond	Bond Length (Å)	ICOHP (eV)
KAO-CO	KAO-H_{11}…O_{39}-CO	1.83	−0.67
	KAO-H_{14}…O_{38}-COOH	1.88	−0.55
KAO-COOH	KAO-H_{16}…O_{38}-COOH	1.75	−0.88
	KAO-H_{4}…O_{39}-CO	1.81	−0.76
	KAO-H_{6}…O_{38}-COOH	1.96	−0.43
	KAO-O_{34}…H_{25}-COOH	1.98	−0.66
KAO-F	KAO-H_{11}…F	2.22	−0.20

Acknowledgement

This study was supported by the National Natural Science Foundation of China (No. 41472231).

References

Alvarez-Esmorís C, Conde-Cid M, Fernández-Sanjurjo MJ, et al. 2021. Environmental relevance of adsorption of doxycycline, enrofloxacin, and sulfamethoxypyridazine before and after the removal of organic matter from soils. Journal of Environmental Management, 287: 112354. DOI：10.1016/j.jenvman.2021.112354.

Borden D, Giese RF. 2001. Baseline studies of the clay minerals society source clays: Cation exchange capacity measurements by the ammonia-electrode method. Clays And Clay Minerals, 49(5): 444−445. DOI：10.1346/CCMN.2001.0490510.

Chassé AW, Ohno T, Higgins SR, et al. 2015. Chemical force spectroscopy evidence supporting the Layer-by-Layer model of organic matter binding to Iron (oxy) Hydroxide mineral surfaces. Environmental Science & Technology, 49(16): 9733−9741. DOI：10.1021/acs.est.5b01877.

Cheng W, Li JB, Sun J, et al. 2023. Nalidixic Aacid and Fe(II)/Cu(II) coadsorption at Goethite and Akaganeite surfaces. Environmental Science & Technology, 57(41): 15680−15692. DOI：10.1021/acs.est.3c05727.

Deogratias G, Al-Qurashi OS, Wazzan N. 2023. Optical and electronic properties enhancement via chalcogenides: Promising materials for DSSC applications. Journal of Molecular Modeling, 29(4): 86. DOI：10.1007/s00894-023-05472-0.

Gao JA, Pedersen JA. 2005. Adsorption of sulfonamide antimicrobial agents to clay minerals. Environmental Science & Technology, 39(24): 9509−9516. DOI：10.1021/es050644c.

George J, Petretto G, Naik A, et al. 2022. Automated bonding analysis with crystal orbital hamilton populations. Chempluschem, 87(11): e202200123. DOI：10.1002/cplu.202200123.

Guaita DP, Sayen S, Boudesocque S, et al. 2011. Copper(II) influence on flumequine retention in soils: Macroscopic and molecular investigations. Journal of Colloid and Interface Science, 357(2): 453−459. DOI：10.1016/j.jcis.2011.01.097.

Hacıosmanoğlu GG, Mejías C, Martín J, et al. 2022. Antibiotic adsorption by natural and modified clay minerals as designer adsorbents for wastewater treatment: A comprehensive review. Journal of Environmental Management, 317: 115397. DOI：10.1016/j.jenvman.2022.115397.

Han YH, Liu WL, Zhou J, et al. 2016. Interactions between kaolinite Al-OH surface and sodium hexametaphosphate. Applied Surface Science, 387: 759−765. DOI：10.1016/j.apsusc.2016.07.002.

Hu JS, Xiao HY, Tang XY, et al. 2025. Polarity and fluorescent fractions of manure dissolved organic matter could affect differently the adsorption and desorption of antibiotics in soils. Journal of Environmental Management, 378: 124767. DOI：10.1016/j.jenvman.2025.124767.

Ke Y, Zhu X, Si S, et al. 2023. A novel adsorbent of Attapulgite & Carbon composites derived from spent bleaching earth for synergistic removal of copper and tetracycline in water.

International Journal of Environmental Research and Public Health, 20(2): 1573. DOI: 10.3390/ijerph20021573.

Khalid S, Shahid M, Natasha Shah AH, et al. 2020. Heavy metal contamination and exposure risk assessment via drinking groundwater in Vehari, Pakistan. Environmental Science and Pollution Research, 27(32): 39852−39864. DOI: 10.1007/s11356-020-10106-6.

Khandal RK, Thoisydur JC, Terce M. 1991. Adsorption characteristics of flumequine on Kaolinitic clay. Geoderma, 50(1-2): 95−107. DOI: 10.1016/0016-7061(91)90028-r.

Li YD, Bi EP, Chen HH. 2017. Sorption behavior of ofloxacin to kaolinite: Effects of pH, ionic strength, and Cu(II). Water, Air, & Soil Pollution, 228(1): 46. DOI: 10.1007/s11270-016-3236-x.

Luo T, Le CS, Luong NT, et al. 2024. Goethite-bound copper controls the fate of antibiotics in aquatic environments. Environmental Science & Technology Water, 4(2): 638−647. DOI: 10.1021/acsestwater.3c00666.

Ma J, Xiong Y, Dai X, et al. 2020. Coadsorption behavior and mechanism of ciprofloxacin and Cu(II) on graphene hydrogel wetted surface. Chemical Engineering Journal, 380: 122387. DOI: 10.1016/j.cej.2019.122387.

Maged A, Iqbal J, Kharbish S, et al. 2020. Tuning tetracycline removal from aqueous solution onto activated 2: 1 layered clay mineral: Characterization, sorption and mechanistic studies. Journal of Hazardous Materials, 384: 121320. DOI: 10.1016/j.jhazmat.2019.121320.

Nguyen AQ, Nguyen ATQ, Nguyen NTM, et al. 2023. Sorption of oxytetracycline to micro-sized colloids under concentrated salt solution: A perspective on terrestrial-to-ocean transfer of antibiotics. Science of the Total Environment, 905: 167005. DOI: 10.1016/j.scitotenv.2023.167005.

Ortiz-Ramos U, Leyva-Ramos R, Mendoza-Mendoza E, et al. 2022. Removal of tetracycline from aqueous solutions by adsorption on raw Ca-bentonite. Effect of operating conditions and adsorption mechanism. Chemical Engineering Journal, 432: 134428. DOI: 10.1016/j.cej.2021.134428.

Pantaleone S, Rimola A, Sodupe M. 2020. Canonical, deprotonated, or zwitterionic? II. A computational study on amino acid interaction with the TiO2 (110) rutile surface: Comparison with the anatase (101) surface. Physical Chemistry Chemical Physics, 22(29): 16862−16876. DOI: 10.1039/d0cp01429j.

Urbaniak B, Kokot ZJ. 2009. Analysis of the factors that significantly influence the stability of fluoroquinolone-metal complexes. Analytica Chimica Acta, 647(1): 54−59. DOI: 10.1016/j.aca.2009.05.039.

Wang B, Lin J, Hu QC, et al. 2023. Adsorption of oxytetracycline on subalpine meadow soil from Zoige Plateau, China: Effects of the coexisting Cu^{2+}. Environmental Research, 231: 116221. DOI: 10.1016/j.envres.2023.116221.

Wang WJ, Nan ZJ, Kong WC, et al. 2025. Enhanced adsorption and leaching behavior of fluoroquinolone antibiotics in soil amended with cattle manure under varying rainfall condition. Journal of Environmental Chemical Engineering, 13(3): 116831. DOI: 10.1016/j.jece.2025.116831.

Xiong HX, Zhao XJ, Song K, et al. 2024. Cow manure pellet biochar: Leaching of Cu(II) and its corresponding influences on tetracycline adsorption. Water, Air & Soil Pollution, 235(4): 255. DOI: 10.1007/s11270-024-07045-0.

Xu YG, Yu WT, Ma Q, et al. 2015. Interactive effects of sulfadiazine and Cu(II) on their sorption and desorption on two soils with different characteristics. Chemosphere, 138: 701−707. DOI: 10.1016/j.chemosphere.2015.07.049.

Xu ZS, Huang WY, Xie HJ, et al. 2021a. Co-adsorption and interaction mechanism of cadmium and sulfamethazine onto activated carbon surface. Colloids and Surfaces a-Physicochemical and Engineering Aspects, 619: 126540. DOI: 10.1016/j.colsurfa.2021.126540.

Xu ZW, Lv SQ, Hu SX, et al. 2021b. Effect of soil solution properties and Cu^{2+} co-existence on the adsorption of sulfadiazine onto paddy soil. International Journal of Environmental Research and Public Health, 18(24): 13383. DOI: 10.3390/ijerph182413383.

Xue M, Gu X, Qin Y, et al. 2022. Enantioselective behavior of flumequine enantiomers and metabolites' identification in sediment. Journal of Analytical Methods in Chemistry, 2022: 1−12. DOI：10.1155/2022/2184024.

Yu F, Li Y, Huang GQ, et al. 2020. Adsorption behavior of the antibiotic levofloxacin on microplastics in the presence of different heavy metals in an aqueous solution. Chemosphere, 260: 127650. DOI：10.1016/j.chemosphere.2020.127650.

Zainab SM, Junaid M, Rehman MYA, et al. 2021. First insight into the occurrence, spatial distribution, sources, and risks assessment of antibiotics in groundwater from major urban-rural settings of Pakistan. Science of the Total Environment, 791: 148298. DOI：10.1016/j.scitotenv.2021.148298.

Zhang ZJ, Yuan ZT, Zhuang L, et al. 2021. Adsorption mechanism of polyacrylamide on kaolinite surface in the presence of Ca^{2+}: Insights from DFT calculation. Chemical Physics Letters, 776: 138672. DOI：10.1016/j.cplett.2021.138672.

Zhao N, Ju F, Song QW, et al. 2022. A simple empirical model for phenanthrene adsorption on soil clay minerals. Journal of Hazardous Materials, 429: 127849. DOI：10.1016/j.jhazmat.2021.127849.

Zhao YP, Gu XY, Li SY, et al. 2015. Insights into tetracycline adsorption onto kaolinite and montmorillonite: Experiments and modeling. Environmental Science and Pollution Research, 22(21): 17031−17040. DOI：10.1007/s11356-015-4839-2.

Zhao Z, Lin S, Yu Z, et al. 2023. Facile synthesis of triazine-based microporous organic network for high-efficient adsorption of flumequine and nadifloxacin: A comprehensive study on adsorption mechanisms and practical application potentials. Chemosphere, 315: 137731. DOI：10.1016/j.chemosphere.2022.137731.

Zhao ZC, Yang CL, Cao ZX, et al. 2025. Rational design of MoS_2/$MoSe_2$ lateral heterostructure with optimal component ratio used for high-efficient photocatalytic overall water splitting. Surfaces and Interfaces, 56: 105513. DOI：10.1016/j.surfin.2024.105513.